# Signatures of superconducting gap inhomogeneities in optical properties

J. P. F. LeBlanc[*] and E. J. Nicol

*Department of Physics, University of Guelph, Guelph, Ontario, Canada N1G 2W1*
*and Guelph-Waterloo Physics Institute, University of Guelph, Guelph, Ontario, Canada N1G 2W1*

J. P. Carbotte

*Department of Physics and Astronomy, McMaster University, Hamilton, Ontario, Canada L8S 4M1*
*and Canadian Institute for Advanced Research, Toronto, Ontario, Canada M5G 1Z8*

Scanning tunneling spectroscopy applied to the high-$T_c$ cuprates has revealed significant spatial inhomogeneity on the nanoscale. Regions on the order of a coherence length in size show variations of the magnitude of the superconducting gap of order $\pm 20\%$ or more. An important unresolved question is whether or not these variations are also present in the bulk, and how they influence superconducting properties. As many theories and data analyses for high-$T_c$ superconductivity assume spatial homogeneity of the gap magnitude, this is a pressing question. We consider the far-infrared optical conductivity and evaluate, within an effective-medium approximation, what signatures of spatial variations in gap magnitude are present in various optical quantities. In addition to the case of $d$-wave superconductivity, relevant to the high-$T_c$ cuprates, we have also considered $s$-wave gap symmetry in order to provide expected signatures of inhomogeneities for superconductors in general. While signatures of gap inhomogeneities can be strongly manifested in $s$-wave superconductors, we find that the far-infrared optical conductivity in $d$-wave is robust against such inhomogeneity, such that any changes maintain the character of a curve for a single $d$-wave gap.

PACS number(s): 74.25.Gz, 74.72.−h, 74.40.+k

## I. INTRODUCTION

There is considerable evidence from scanning tunneling microscopy (STM) that some cuprates are intrinsically inhomogeneous on the nanoscale. While $Bi_2Sr_2CaCu_2O_{8+\delta}$ (BSCCO) has been extensively studied,[1–8] spatial inhomogeneities exist as well in $La_{2-x}Sr_xCuO_4$ (Ref. 9) and in electron doped systems such as $Pr_{0.88}LaCe_{0.12}CuO_4$.[10] On the other hand, the inhomogeneities seen in STM can be affected through sample preparation methods.[11] A critical question is whether these inhomogeneities exist only on the surface layer to which STM is sensitive, or are also present in the bulk. Evidence that they are not present in the bulk is provided by NMR data on $YBa_2Cu_3O_{7-\delta}$ (YBCO).[12] Also, Loram *et al.*[13] have argued that, even in BSCCO, bulk inhomogeneities on the scale indicated in STM experiments are inconsistent with specific-heat data; although this view has been challenged recently by Andersen *et al.*[14] who concluded that nanoscale inhomogeneity in BSCCO is a bulk property. In view of this conflict, it is clearly important to look for other possible probes of bulk nanoscale variation. Such a probe is infrared absorption. In this paper, we consider the effect of nanoscale regions on optical properties with an aim at identifying their signatures in these quantities.

To understand how nanoscale variations of the superconducting energy gap can affect optical properties, we have applied an effective-medium approximation (EMA) to an inhomogeneous system with a distribution of superconducting energy gaps. The merit of this approach is that we do not commit ourselves to any particular microscopic model of the inhomogeneity, but rather examine the macroscopic electrodynamics with a minimum of assumptions. In order to consider the case of the high-$T_c$ superconductors, we include $d$-wave gap symmetry in our calculations and model the gap distribution based on BSCCO STM gap maps of Refs. 2 and 6. As can be seen in these and other references, using STM to image a surface allows for mapping of high and low regions of superconducting gap magnitude, $\Delta$.

The lattice structure of the BSCCO compounds is such that the surface can cleave smoothly between adjacent Bi-O planes, resulting in what should be a uniform surface structure. However, despite the supposed uniform lattice structure—that is to say there is no evidence of restructuring on the surface after cleaving—there is a spatially inhomogeneous energy gap structure at the surface. These inhomogeneous gap structures are commonly displayed in the form of a gap map, as seen in Fig. 1(a). In this figure, the blue patches are regions with a gap magnitude of about 50 meV and the red have gap values of about 20 meV. The largest number of regions occurs with a gap of $\sim 32$ meV and the variation away from this value is about $\pm 20\%$ as indicated in Fig. 1(c). The diameters of these regions are typically of order 3 nm,[7] but there is no particular pattern or underlying structure, rather the regions appear to be randomly distributed.

It is also important to note the discontinuous nature of these gap maps, as can be seen in Fig. 2, where a scan along a line across the surface is shown. Here we see that the gap map contains distinct regions with nearly uniform gap values and consequently does not represent a smoothly varying single-gap function $\Delta(x)$, but rather suggests separate patches, each with its own gap value.

In implementing the EMA as a phenomenological model, we are assuming that these STM images directly reflect the bulk gap distribution in an attempt to find signatures of this gap inhomogeneity. However, in the following, our results for far-infrared optical conductivity will show that no strong signatures were observed in mixtures of $d$-wave supercon-
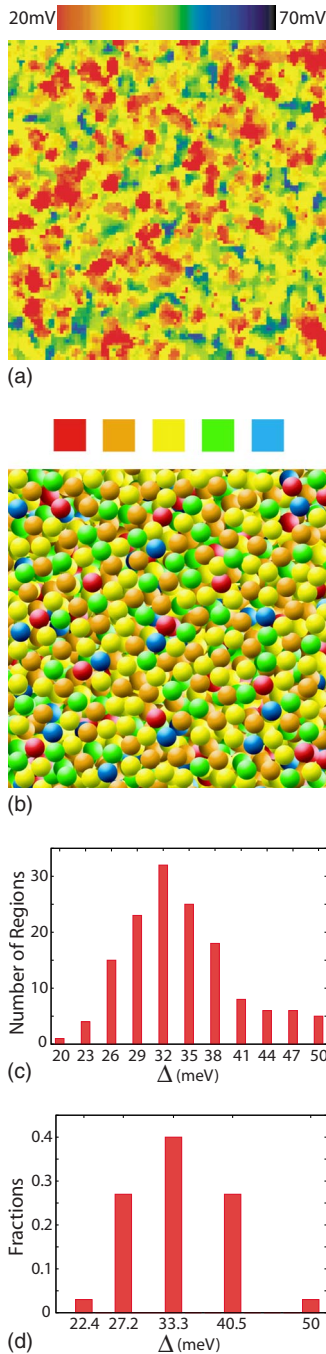
(a)

(b)

(c)

(d)

FIG. 1. (Color online) (a) STM gap map of surface of over-doped (OD) BSCCO with $T_c=89$ K from Refs. 2 and 6. (b) Schematic of system comprised of spherical particles distributed at random as dictated by histogram (d). (c) Histogram of gap distribution shown in (a) adapted from Ref. 2. (d) Rebinning of histogram (c) to a set of five gaps.
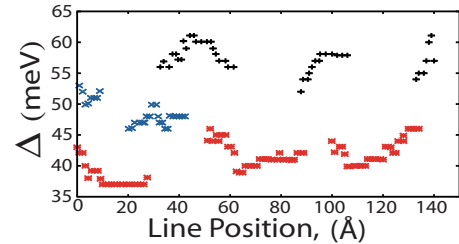


FIG. 2. (Color online) Adapted from Ref. 2. Plot of superconducting gap value as a function of position along a straight line of an STM gap map.

On the other hand, we find that signatures in mixtures of *s*-wave superconductors present themselves in the form of a distribution of gap onsets over the range of gaps. This distribution results in an optical conductivity and optical self-energy which are distinct from a single-gap system, and that are highly dependent upon the range of variation in the gap as well as the actual distribution present.

In Sec. II, we begin by presenting the theory for the EMA and its use to obtain the optical conductivity. In Sec. III, we will present our results for *d*-wave superconductivity based on the distribution of gaps seen in STM. Section IV will then present results for *s*-wave superconductivity, and we summarize our conclusions in Sec. V.

## II. EFFECTIVE-MEDIUM THEORY

It is of interest to us to understand in which systems and on what energy scales we might expect to see indications of inhomogeneities in bulk optical properties in order to make generalizations on, or identify, inhomogeneities in new materials. For this reason, we seek a purely phenomenological method of examining these effects, and here we will turn to Bruggeman's EMA.[15,16] This EMA has been rigorously tested and previously applied to both microscopic metallic and microscopic superconducting-normal mixtures.[17–21] It has also been used more recently to model[22,23] the very low frequency optical response in the cuprates and to discuss, in particular, the THz data on BSCCO from Corson *et al.*[24,25] In certain circumstances, an alternative choice of EMA might be used, the Maxwell-Garnet EMA,[16] however, that EMA applies when there are a dilute set of regions embedded in a large uniform background, which is not the case seen here in the STM of Fig. 1(a). In the following, we wish to make a semiclassical approximation, treating the system classically as having randomly distributed regions, each a uniform superconducting material, with properties defined by nonclassical BCS results. The implicit assumption here is the randomness of the distribution of regions, since it has yet to be understood how and if these inhomogeneities are distributed throughout the bulk material.

For understanding the optical response of the entire system, we now summarize the idea of the EMA. An electromagnetic wave, of frequency $\omega$, moving through a composite material will undergo multiple scattering and absorption events. In a bulk material these events are accounted for as an average by means of an effective complex dielectric func-

ductors and indeed the results of the EMA can be very well approximated by a single spatially averaged gap value, which provides support for the past and continuing use of theories and data analyses which assume a spatially homogeneous energy gap in the bulk of high-$T_c$ superconductors. It would appear from our work that even if the inhomogeneities are present in the bulk, this assumption will be robust.

tion $\epsilon_m(\omega)$. If the bulk material is a composite, it is assumed to be composed of a number of regions of uniform dielectric functions $\epsilon_i(\omega)$. The scattering caused by these regions is dependent upon both the shape and size of the regions (grains). These scattering events can be taken into account by allowing each grain to become polarized, producing its own additional field. When we extend this to a macroscopic system, we add the constraint that the entire material should have a zero net polarization, i.e.,[20]

$$\sum_i f_i P_i = 0, \tag{1}$$

where $f_i$ is the relative fraction of the occurrence of a certain type of grain indexed by $i$ and $P_i$ is that constituent's polarization. Knowing this, we can solve for the real and imaginary parts of $\epsilon_m(\omega)$ in the following equation:

$$\sum_i f_i \frac{(\epsilon_i - \epsilon_m)}{g\epsilon_i + (1-g)\epsilon_m} = 0, \tag{2}$$

where $g$ is the depolarization factor, determined by the shape of the constituent grain.[16,17] The form of the polarization in Eq. (2) can be seen as the electric dipole contribution of a multipole expansion. Subsequent terms in the polarization (magnetic dipole, electric quadrupole, etc.) scale as functions of the grain size. In the spherical case these terms scale as $(\omega R_i/c)^2 = (R_i/\lambda)^2$, where $R_i$ is the radius of the individual grains and $\lambda$ is the wavelength of the field. For this case, the correction to Eq. (2) to next order would be

$$\sum_i f_i \left[ \frac{(\epsilon_i - \epsilon_m)}{\epsilon_i + 2\epsilon_m} + \frac{1}{30}\left(\frac{\omega R_i}{c}\right)^2 (\epsilon_i - \epsilon_m) \right] = 0. \tag{3}$$

We can see certain limits where the second term can be neglected. In the small grain limit, we would expect the far-infrared (long wavelength limit) response to be completely dominated by the first term. As this is the region of interest for detecting signatures of the superconducting energy gap, the EMA as in Eq. (2), with $g$ set to a value of 1/3 (spherical grains), is appropriate for our purpose. Note that we do not find any qualitative differences in the calculations reported here for other typical values of $g$.

To implement the above EMA, we require the frequency dependent complex conductivity $\sigma(\omega) = \sigma_1(\omega) + i\sigma_2(\omega)$ as the dielectric function can be written as $\epsilon(\omega) = \epsilon_\infty + i[4\pi\sigma(\omega)/\omega]$, where $\epsilon_\infty$ is the high frequency dielectric constant. The constituent conductivities that we use for our purpose here are calculated according to Zimmermann et al.[26] for the case of BCS $s$-wave superconductors with variable impurity scattering and according to Schürrer et al.[27] for the BCS $d$-wave case. In this paper, we consider only an elastic scattering rate in the optical conductivity and have not included inelastic scattering, as might arise due to electron-boson interactions, such as phonons and spin fluctuations. For a system of $N$ different types of superconducting grains, the EMA of Eq. (2) can be expanded to the form of an $N$th order complex polynomial in $\epsilon_m(\omega)$ or by setting $\epsilon_k = 1 + i(4\pi\sigma_k/\omega)$ ($k = 1, 2, \ldots, N$ and $m$) as a complex polynomial in $\sigma_m$. For example, in $\epsilon$ we now have

$$\epsilon_m^N(\omega) + a_1 \epsilon_m^{N-1}(\omega) + \cdots + a_N \epsilon_m^0(\omega) = 0, \tag{4}$$

where the coefficients $a_i$ vary based on the choice of $N$. For an $N = 2$ system, one can solve directly for $\epsilon_m$ by substituting in its complex form, $\epsilon_m = \epsilon_{1m} + i\epsilon_{2m}$, and solving for the real and imaginary parts separately. Analytically, this becomes largely unfeasible for $N > 2$. For this reason, considerations of composites, with a large number of constituents, $N$, have not been thoroughly explored. Numerical solutions, however, are much more feasible. All that is required is solving for the set of $a_i$'s for each choice of $N$. This turns out to be a difficult task for $N > 3$ and it is preferable to use a program to solve this algebraically. For example, for the $N = 2$ case,

$$a_1 = \frac{1}{b_0}[-f_1\epsilon_1(\omega)(1-g) + f_1 g\epsilon_2(\omega) - f_2\epsilon_2(\omega)(1-g) + f_2 g\epsilon_1(\omega)], \tag{5}$$

$$a_2 = \frac{1}{b_0}[-f_1\epsilon_1(\omega)g\epsilon_2(\omega) - f_2\epsilon_2(\omega)g\epsilon_1(\omega)], \tag{6}$$

where $b_0 = 1 - g$. We can see that these coefficients depend on the dielectric function $\epsilon_i(\omega)$ (or conductivity) of each constituent, as well as their relative volume fractions $f_i$ and the depolarization factor, $g$. These are the key pieces of information required to perform such an effective-medium calculation, and as such, will be explained in detail for each case we wish to examine. Knowing the numerical coefficients, $a_i$ in Eq. (4), reduces the EMA calculation to the problem of numerically solving an $N$th order complex polynomial. Such a polynomial has $N$ solutions, of which only one is generally completely physical as $\epsilon_2(\omega)$ must be strictly positive for each choice of $\omega$.

## III. $d$-WAVE ENERGY GAP INHOMOGENEITIES

In order to determine possible signatures in the bulk due to the inhomogeneities seen by STM, we created a mixture of superconducting patches which is motivated by Fig. 1(a) and shown schematically in Fig. 1(b). We tried to maintain the same gap distribution seen in experiment and shown in the histogram of Fig. 1(c), but have rebinned the distribution so that it gives only five fractions $f_i$ in order to reduce the complexity of the numerical calculation. This is shown in Fig. 1(d). Furthermore, we assumed that each constituent has $d$-wave gap symmetry similar to what one would expect in the bulk BSCCO conductivity[28] and have used the BCS $d$-wave conductivity program of Ref. 27 to provide the input conductivities to the EMA. The BCS conductivity, while missing the inelastic component, does exhibit similar qualitative features as seen in experimental results, and can be applied with a minimal number of parameters: the energy gap $\Delta$, the plasma frequency $\omega_p$, the temperature $T$, and the scattering parameter $t^+ = 1/(2\pi\tau)$, where $1/\tau$ is the elastic scattering rate. Since we are interested in the effects of varying only the gap parameter and we wish to limit the parameter space, we compute the EMA using constituents with similar plasma frequencies and scattering rates, but a range of $\Delta$ values. The real part of the input conductivities of the
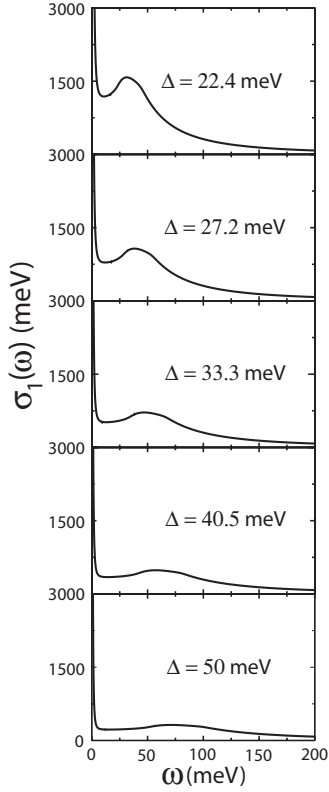
FIG. 3. The real part of the optical conductivity for a $d$-wave superconductor at $T=20$ K for different gap values chosen to match those in the rebinned gap map histogram [Fig. 1(d)]. The curves shown here have $\omega_p=2$ eV and $t^+=0.2$ meV.

constituent superconducting grains is shown in Fig. 3. These curves were calculated with realistic parameters, as given in Ref. 27, i.e., $\omega_p=2$ eV, $t^+=0.2$ meV, at $T=20$ K.

The overall characteristics of the resulting EMA in this case (shown in Fig. 4) remain what would be expected of a single-gap $d$-wave superconductor with scattering in the clean limit. Indeed, if we superimpose the conductivity curve for the average gap value, which dominates the gap distribution seen in STM, we find that there is not much difference between the two curves and therefore we conclude from
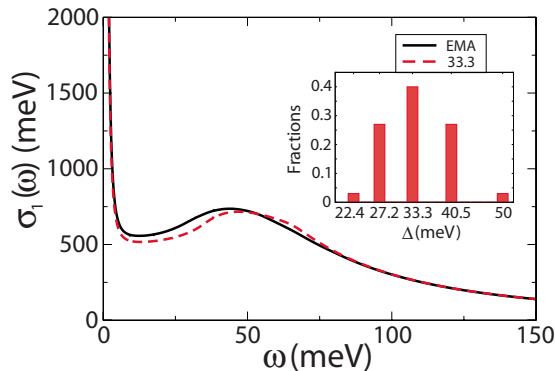


FIG. 4. (Color online) Solid black line: EMA calculation involving constituents described in Fig. 3 with volume fractions from Fig. 1(c) (also shown as an inset here). Dashed red curve: an overlay of the $\Delta=33.3$ meV curve of Fig. 3 for comparison.

these calculations that even if the inhomogeneity persists throughout the bulk, the size of variation in the gap, on scales seen in STM, cause very little variation in the overall conductivity of the sample from that of a single-gap system, and therefore it would be difficult to determine the presence of inhomogeneities from bulk far-infrared optical measurements. Because these superconductors are believed to be in the clean limit the effective variation in superfluid density included in these curves are small. This is very different from the model of Barabash and Stroud[23] where they have found large changes in absorption in the microwave and terahertz region in a model with comparatively very large variation in superfluid density. Likewise, in this region other theoretical works have found mechanisms for inducing large absorption due to inhomogeneity via Josephson coupled grains[29] (not included in our work) or quenched disorder incorporating normal state regions and favoring anticorrelation between the superconducting and normal state inhomogeneity for maximum effect.[30,31] If we add normal regions to our calculation then enhanced absorption will indeed occur at very low frequency and this has been known for some time for two-grain mixtures of normal regions and regions of $s$-wave superconductor. We stress that our work is about imprints of the inhomogeneities on the infrared region and not the terahertz region where, in the latter case, large effects have been seen in experiment over a range of doping.[32] Furthermore, we are taking as input the distribution of gaps suggested by the observation of STM, which are taken to be static. The motivation and the questions that we have asked are different from these other works and we are focused on the region of the energy gap where one might expect to see the effects due to the gap distributions seen in STM.

Further to our discussion of our results in Fig. 4, we note that variation in scattering rates of constituent grains (of up to a factor of 10) does not change the qualitative results of an EMA mixture with $d$-wave symmetry. We do not expect to have large values of the scattering rate, as this would quench the superconducting state, and there is no evidence from STM or otherwise for normal regions mixed in among the regions of inhomogeneous superconductivity at low temperatures. We conclude that the narrow range of gap values seen in STM coupled with the rather smooth nature of the conductivity for a BCS $d$-wave superconductor makes the observation of possible gap inhomogeneities uncertain through far-infrared optics. Adding in realistic inelastic scattering would not change this conclusion as this type of scattering will not introduce new sharp features in the conductivity. As a final point, most approaches to calculating optical properties of the cuprates assume a homogeneous model. Our results indicate that it is appropriate to compare results of such calculations for the average gap with experiment, and that ignoring inhomogeneities is a valid first approximation.

## IV. $s$-WAVE ENERGY GAP INHOMOGENEITIES

With the knowledge of Sec. III, we are now motivated to find possible systems where gap inhomogeneities could have a clear signature in optics and indeed, it is clear that a system with a conductivity curve which contains sharp features
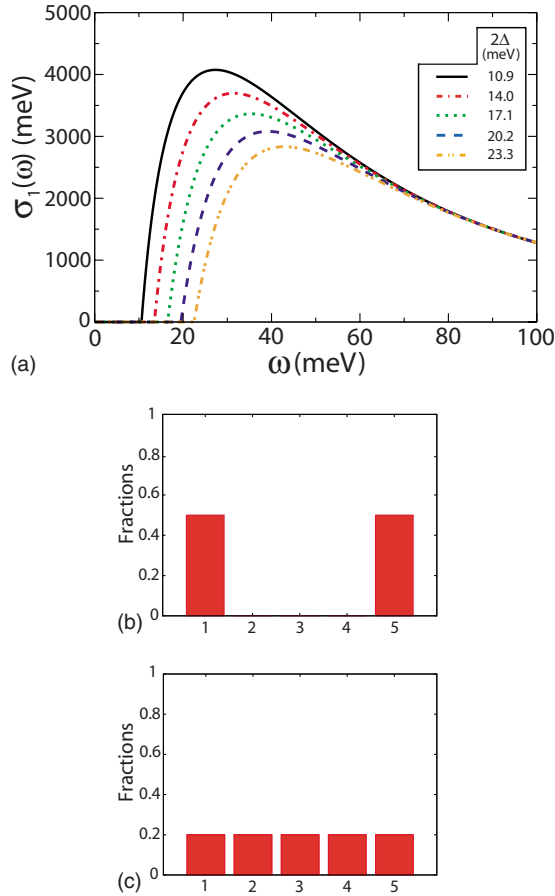
FIG. 5. (Color online) (a) Real part of the conductivity for different values of the energy gap $\Delta$, as discussed in the text. (b) Histogram of two-grain mixture. (c) Histogram of five-grain mixture. ($1 \rightarrow 5$ refer to lowest to highest gap values.)
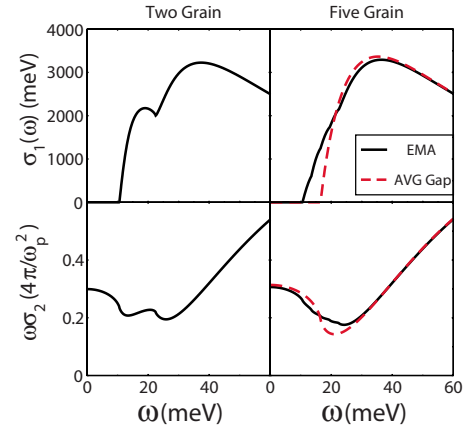


FIG. 6. (Color online) EMA result for two-grain (left) and five-grain (right) composites determined from the histograms in Figs. 5(b) and 5(c). The dashed red curve is the single-gap calculation using the average gap value of the distribution.

would be an ideal candidate. Consequently, we now examine the effect of a distribution of gaps on a conventional $s$-wave BCS superconductor. We begin by calculating the zero temperature BCS $s$-wave conductivities for two simple distributions of gap values shown in Figs. 5(b) and 5(c). We have assumed a constant elastic scattering rate $1/\tau = 50$ meV, and plasma frequency $\omega_p = 2$ eV for all grains and this puts the system in the regime where $2\Delta < 1/\tau$, which is a mildly dirty limit. We calculate this EMA mixture under the assumption that each constituent maintains the same overall transition temperature, therefore, variations in $\Delta$ value can be seen as analogous to changing the $\frac{2\Delta}{T_c}$ ratio from $3.53 \rightarrow 7.53$ in steps of 1. Curves for the real part of the conductivity, used for input to the EMA, are shown in Fig. 5(a).

In the two-grain composite, Fig. 6 (left column), we observe that the separation of gap onsets is sufficient to clearly display a two-gap result in the real part of the conductivity, $\sigma_1$ (top frame). The real part of the conductivity rises sharply out of zero as it does in all of the curves in Fig. 5(a). This is followed by a first peak, after which a second rise begins at twice the value of the largest gap in our two-gap distribution. A second peak follows at higher energy before the normal state Drude form is recovered. This is fundamentally different from, and should not be confused with, a two-band su-

perconductor such as $MgB_2$.[33] It should be noted that the EMA is distinct in this two-gap system from a fractional average of its constituents since both $\sigma_{1m}$ and $\sigma_{2m}$ depend on both the real and imaginary parts of the constituents. In other words, for a two component mixture labeled $a$ and $b$, where $\sigma_a = \sigma_{1a} + i\sigma_{2a}$ and $\sigma_b = \sigma_{1b} + i\sigma_{2b}$, the EMA results in $\sigma_{1m} = \sigma_{1m}(\sigma_{1a}, \sigma_{2a}, \sigma_{1b}, \sigma_{2b})$ and $\sigma_{2m} = \sigma_{2m}(\sigma_{1a}, \sigma_{2a}, \sigma_{1b}, \sigma_{2b})$. This additional dependence of the real part of the conductivity on the imaginary parts of its constituents in general leads to an increased low frequency contribution to $\sigma_{1m}$ from the imaginary conductivities (physically seen as scattering from constituents). The imaginary part multiplied by $\omega$, namely, $\omega\sigma_2(\omega)$, is shown in the lower left panel. As the frequency goes to zero, we find the inverse square of the London penetration depth for the composite system. At finite frequency, there are structures in $\omega\sigma_2(\omega)$ corresponding to the frequencies of the onset of absorption of each of the two grains included in the model. These structures would be easily identifiable.

When we consider a less-separated five-grain distribution [seen in Fig. 5(c), with results in Fig. 6 (right column)], we immediately recognize the loss of clear onset points for each gap value and instead see a broadened rise in $\sigma_1(\omega)$ (Fig. 6, top right frame), which quickly rejoins an average gap fit at frequencies just above the highest $2\Delta$ point. Shown here is the EMA calculation as the solid black curve with the dashed red curve being the calculation for a single-gap system using the average gap of the distribution as the input gap. It is clear that in this more realistic case the signature of inhomogeneities is not as readily identifiable as for the two-gap case. This is also true for the imaginary part, $\omega\sigma_2(\omega)$, shown in the lower frame; now a single minimum is seen similar to the single-gap case, but somewhat more broadened.

The real and imaginary parts of the conductivity are not the only optical quantities that enter a more modern discussion of the subject. In fact, it has been found to be very useful to introduce an optical self-energy $\Sigma^{op}(\omega)$ defined in terms of the generalized Drude formula for the optical conductivity, $\sigma(\omega)$, which is written as[34–36]

$$\sigma(\omega) = \iota \frac{\omega_p^2}{4\pi} \frac{1}{\omega - 2\Sigma^{\text{op}}(\omega)}. \qquad (7)$$

Here $\omega_p$ is the plasma frequency and $\Sigma^{\text{op}}(\omega)$ has both a real and imaginary part related, respectively, to a frequency dependent optical effective mass, $m_{\text{op}}^*(\omega)/m$, (where $m$ is the bare electron mass) and scattering rate, $1/\tau^{\text{op}}(\omega)$, given by

$$\omega \left[ \frac{m_{\text{op}}^*(\omega)}{m} - 1 \right] = -2\Sigma_1^{\text{op}}(\omega) \qquad (8)$$

and

$$\frac{1}{\tau^{\text{op}}(\omega)} = -2\Sigma_2^{\text{op}}(\omega). \qquad (9)$$

An optical mass renormalization parameter, $\lambda^{\text{op}}(\omega)$, is then defined by $m_{\text{op}}^*(\omega)/m = 1 + \lambda^{\text{op}}(\omega)$. These quantities are analogous, but different from, the quasiparticle mass renormalization and scattering rate which follow from the quasiparticle self-energy $\Sigma^{\text{qp}}(\omega)$. Instead, $\Sigma^{\text{op}}(\omega)$ is a two-particle quantity.[37] It is related to the Kubo formula for the current-current correlation function which determines $\sigma(\omega)$.

In general, as stated, the optical and quasiparticle mass renormalization and scattering rate are not the same, although in some limits they can be. As an example, the zero-frequency mass renormalization $\lambda^{\text{op}}(\omega=0)$ and $\lambda^{\text{qp}}$ are equal. In the end, of course, $\Sigma^{\text{op}}(\omega)$ contains exactly the same information as does $\sigma(\omega)$. In fact, one can solve for $1/\tau^{\text{op}}$ and $\lambda_{\text{op}}$ in terms of $\sigma_1$ and $\sigma_2$ to find[34,35]

$$\frac{1}{\tau_{\text{op}}} = \frac{\omega_p^2}{4\pi} \frac{\sigma_1(\omega)}{\sigma_1^2(\omega) + \sigma_2^2(\omega)} \qquad (10)$$

and

$$1 + \lambda_{\text{op}} = \frac{\omega_p^2}{4\pi\omega} \frac{\sigma_2(\omega)}{\sigma_1^2(\omega) + \sigma_2^2(\omega)}. \qquad (11)$$

This does not mean, however, that these quantities have no particular value of their own. It is well documented that they can speak more directly to certain questions than can $\sigma$ itself. For example, $1/\tau^{\text{op}}(\omega)$ provides information on absorption and, in an $s$-wave superconductor, at zero temperature it is zero for photon energies, $\omega$, less than twice the gap. A coherence peak is seen above this energy and at high $\omega$ we recover a measure of the normal state elastic scattering. Further, it has recently been found that in the underdoped cuprates, the real part of $\Sigma^{\text{op}}(\omega)$ possesses a "hatlike" structure which extends in energy over a range of about twice the pseudogap energy. This characteristic structure, which is superimposed on a large smooth incoherent background, is nevertheless unmistakable and provides a direct image of pseudogap formation[38] as it enters the in-plane optical data. By contrast, the effect of the opening of a pseudogap in the real and imaginary part of the conductivity is much more subtle and is spread over a much larger energy range. Thus, the optical quantities defined in Eqs. (10) and (11) have proved useful and here we will consider how they are changed in the case of a distribution of regions of distinct gap values.
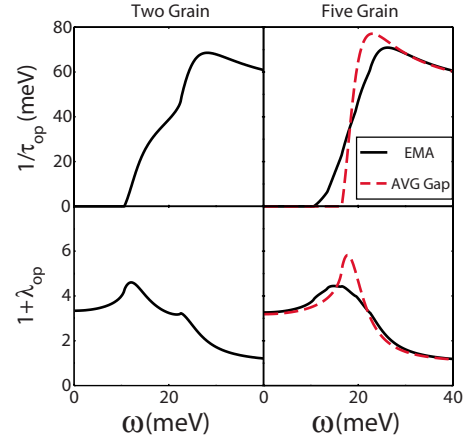


FIG. 7. (Color online) EMA result for the theoretical self-energy of the two-grain (left) and five-grain (right) composite determined by histograms in Figs. 5(b) and 5(c), respectively. The top row shows the scattering rate, $1/\tau^{\text{op}}$, and the bottom row shows the mass renormalization, $1 + \lambda_{\text{op}}$.

In the top row of Fig. 7 we show results for $1/\tau^{\text{op}}(\omega)$ (solid black curve) in meV as a function of $\omega$ (also in meV) for the two- and five-gap distributions of Figs. 5(b) and 5(c). The onset of absorption starts at the lowest value of twice the gap which is roughly 11 meV in our model. Also shown for comparison (dashed red curve) are results for the case of a homogeneous superconductor with the same average gap value. We see that, by comparison, the rise in $1/\tau^{\text{op}}(\omega)$ in the inhomogeneous case, is not as steep and proceeds more gradually, being spread out over an energy scale which corresponds to the spread in gap values in our model distribution. The peak in the red dashed curve has its origin in the well-known coherence peak of the BCS $s$-wave electronic density of states. In the normal state, $1/\tau^{\text{op}}(\omega)$ would be independent of $\omega$ and equal to the input constant impurity scattering rate of 50 meV in this example. This is the value to which $1/\tau^{\text{op}}(\omega)$ (superconducting) tends toward for $\omega$ greater than a few times the gap. In the superconducting state, however, no absorption is possible below twice the gap, at which energy $1/\tau^{\text{op}}(\omega)$ rises sharply and overshoots its normal state value, not because the intrinsic scattering potential has increased but rather because there are more final states available for absorption. For the inhomogeneous case this feature is simply smeared out somewhat because of the distribution of different superconducting regions which are sampled.

In the lower row of Fig. 7 we show our results for the optical mass enhancement parameter $[1 + \lambda_{\text{op}}(\omega)]$ in the two- and five-gap cases. The solid black curve is for the inhomogeneous case and the red dashed curve is the homogeneous case with an averaged gap value for comparison. We note the inhomogeneities smear out the peak in $\lambda_{\text{op}}(\omega)$ around $2\Delta$. However, in all other aspects the curves are similar. We emphasize two points. First, for $\omega$ large compared with the gap, the mass renormalization factor $\lambda_{\text{op}}(\omega)$ tends toward zero, which agrees with its normal state value. At $\omega=0$, however, $\lambda_{\text{op}}$ is seen to be quite large ($\sim 2.5$) in both the homogeneous and inhomogeneous cases. In this limit, the optical effective mass has a very definite meaning. It is the value of the electron mass that one is to give the electrons if one wishes to

use the classical London formula for the penetration depth $\lambda_L$ at $T=0$, namely $\lambda_L^{-2}=4\pi ne^2/m^*c^2$ where $n$ is the free electron density, $e$ is the electron charge and $c$ is the velocity of light. In the clean limit; i.e., no elastic scattering, $m^*$ would be the bare electron mass. Including impurities in BCS theory reduces the London penetration depth and this can be expressed by changing $m$ to $m^*(\omega=0)$ in the conventional expression. Our results show that this result is only slightly changed in the inhomogeneous case; i.e., $m^*(\omega=0)$ is only very slightly larger. The main effect of inhomogeneities manifests itself at finite frequency in the region of twice the gap. We see that, as compared with the dashed red curve, the solid black curve shows a much broader peak which is a direct consequence of spatial gap variations. The peak in $\lambda^{op}(\omega)$ around twice the gap is directly tied to the rapid rise in $1/\tau^{op}(\omega)$ at this same frequency, as these are Kramers-Kronig (KK) related; i.e., a step in the scattering rate at $\omega=2\Delta$ translates into a logarithmic singularity at $2\Delta$ in its KK transform. We note in passing that a recent optical study of MoGe (Ref. 39) has revealed such a smearing of coherence peaks in the thinnest films studied, which could be attributed to inhomogeneities, however, other evidence suggests otherwise. Likewise, a recent optical study on CaC$_6$ found that a fit to a distribution of gaps done as an averaging of $s$-wave conductivity curves was necessary to fit the measured reflectance spectra;[40] however, this distribution is predicted from density-functional calculations and therefore should not be associated with inhomogeneities. It remains to be seen if there will be an example from $s$-wave superconductivity for testing for inhomogeneities as we have seen for the $d$-wave cuprate superconductors. Recent new techniques of imaging the surface of materials optically to see the inhomogeneous evolution of regions of metallic or insulating response[41] may prove to be a promising venue for these studies if the technique can be successfully developed for low enough temperatures to access the superconducting state.

We have shown our result for the $d$-wave conductivity in the clean limit and the $s$-wave case in the dirty limit as these are the regimes in which one finds these systems experimentally. However, in Fig. 8 for comparison, we show the five-grain gap distribution in an EMA for an $s$-wave superconductor in the clean limit where $1/\tau=1$ meV. In this case, one sees considerable structure in the EMA conductivity, even compared to the dirty limit $s$-wave case. This serves to illustrate two points. First, the $d$-wave case is different from the $s$-wave case in this limit. Second, this figure stresses once again that the presence of sharp features in the individual conductivities of the grains will give rise to signatures of inhomogeneities in the bulk conductivity curve. In the clean limit, the $s$-wave conductivity has a steeper rise and a peak at $2\Delta$ as opposed to the dirty limit, and hence the presence of structure appears in the EMA in this case.

## V. SUMMARY AND CONCLUSIONS

Optical absorption is a probe of bulk properties. Using effective-medium theory, we have calculated the far-infrared optical conductivity of a superconductor consisting of a
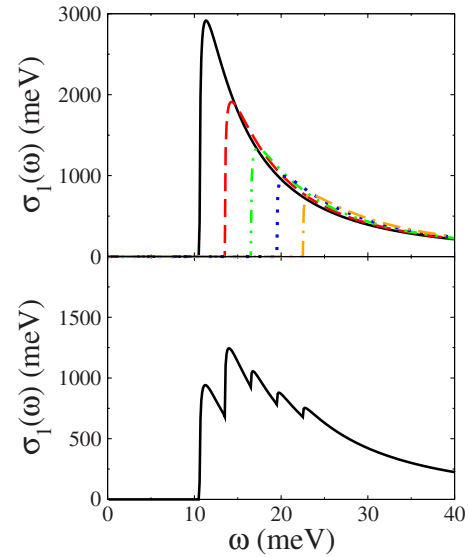


FIG. 8. (Color online) EMA result for an $s$-wave superconductor in the clean limit with a five-grain composite using the same distribution of gaps as given in Fig. 5 but for $1/\tau=1$ meV. The top frame shows the input conductivities with the same line labeling as in Fig. 5(a) and the bottom frame shows the EMA result.

random array of nanoscale regions having different magnitudes of superconducting gap. The superconductivity in each grain is described within a BCS model, and both $s$- and $d$-wave symmetry are considered. For simplicity, models consisting of two and five distinct gap values are examined in detail. For an $s$-wave superconductor, the real part of the optical conductivity is zero for frequencies below twice the gap, with the missing optical spectral weight transferred to the condensate. For $d$-wave, the region below $2\Delta$ is also depleted, although some absorption remains at all frequencies and there is no sharp threshold in $\sigma_1(\omega)$ vs $\omega$. In this latter circumstance the infrared conductivity of the composite system does not exhibit qualitatively different behavior as compared with the single grain which would represent a clear signature of the bulk inhomogeneities. In fact, there are no quantitative differences between $\sigma(\omega)$ of the composite and the individual grains, and the electromagnetic response appears close to that for the average gap. By contrast, for an $s$-wave gap, the sharp absorption edge in $\sigma_1(\omega)$ at twice the gap which is characteristic of a uniform BCS superconductor becomes less steep reflecting the onset of a distribution of gaps rather than of a single one. For a distribution involving only two well-separated gap values, each is seen distinctly in both the real and imaginary parts of the conductivity as well as in the real and imaginary parts of the corresponding optical self-energy. This latter property follows directly from knowledge of the conductivity and has been found useful in past discussions of, for example, boson structures in optical properties. For the case of a distribution of many gap values, the presence of each individual gap is less evident with $\sigma_1(\omega)$ showing rather gradual onset over a frequency range representative of the variation in gap values. In conclusion, signatures of nanoscale spatial inhomogeneities in the far-

infrared optical conductivity are much more readily recognized for composites consisting of *s*-wave gap symmetry components than they are for those with *d*-wave gap symmetry. Indeed, the fact that the *d*-wave case appears to be largely unaffected by the existence of inhomogeneities in spite of their apparent presence in STM gives support for the continued use of single-gap models for calculation and analysis of optical conductivity of the high-$T_c$ cuprates in the far-infrared, which covers the energy region of the superconducting energy gap.

*leblanc@physics.uoguelph.ca

[1] S. H. Pan, J. P. O'Neal, R. L. Badzey, C. Chamon, H. Ding, J. R. Engelbrecht, Z. Wang, H. Eisaki, S. Uchida, A. K. Gupta, K. W. Ng, E. W. Hudson, K. M. Lang, and J. C. Davis, Nature (London) **413**, 282 (2001).

[2] K. M. Lang, V. Madhavan, J. E. Hoffman, E. W. Hudson, H. Eisaki, S. Uchida, and J. C. Davis, Nature (London) **415**, 412 (2002).

[3] C. Howald, H. Eisaki, N. Kaneko, M. Greven, and A. Kapitulnik, Phys. Rev. B **67**, 014533 (2003).

[4] A. C. Fang, L. Capriotti, D. J. Scalapino, S. A. Kivelson, N. Kaneko, M. Greven, and A. Kapitulnik, Phys. Rev. Lett. **96**, 017007 (2006).

[5] K. K. Gomes, A. N. Pasupathy, A. Pushp, S. Ono, Y. Ando, and A. Yazdani, Nature (London) **447**, 569 (2007).

[6] K. McElroy, D. H. Lee, J. E. Hoffman, K. M. Lang, J. Lee, E. W. Hudson, H. Eisaki, S. Uchida, and J. C. Davis, Phys. Rev. Lett. **94**, 197005 (2005).

[7] K. McElroy, J. Lee, J. A. Slezak, D.-H. Lee, H. Eisaki, S. Uchida, and J. C. Davis, Science **309**, 1048 (2005).

[8] A. N. Pasupathy, A. Pushp, K. K. Gomes, C. V. Parker, J. Wen, Z. Xu, G. Gu, S. Ono, Y. Ando, and A. Yazdani, Science **320**, 196 (2008).

[9] T. Kato, S. Okitsu, and H. Sakata, Phys. Rev. B **72**, 144518 (2005).

[10] F. C. Niestemski, S. Kunwar, S. Zhou, S. Li, H. Ding, Z. Wang, P. Dai, and V. Madhavan, Nature (London) **450**, 1058 (2007).

[11] B. W. Hoogenboom, K. Kadowski, B. Revaz, and O. Fischer, Physica C **391**, 376 (2003).

[12] J. Bobroff, H. Alloul, S. Ouazi, P. Mendels, A. Mahajan, N. Blanchard, G. Collin, V. Guillen, and J.-F. Marucco, Phys. Rev. Lett. **89**, 157002 (2002).

[13] J. W. Loram, J. L. Tallon, and W. Y. Liang, Phys. Rev. B **69**, 060502(R) (2004).

[14] B. M. Andersen, A. Melikyan, T. S. Nunner, and P. J. Hirschfeld, Phys. Rev. B **74**, 060501(R) (2006).

[15] D. Bruggeman, Ann. Phys. **24**, 636 (1935).

[16] G. Carr, S. Perkowitz, and D. Tanner, in *Infrared and Millimeter Waves*, edited by K. J. Button (Academic, New York, 1985), Vol. 13, pp. 171–263.

[17] D. Stroud, Phys. Rev. B **12**, 3368 (1975).

[18] D. Stroud and F. P. Pan, Phys. Rev. B **17**, 1602 (1978).

[19] D. Stroud, Phys. Rev. B **19**, 1783 (1979).

[20] R. Landauer, J. Appl. Phys. **23**, 779 (1952).

[21] J. Garner and D. Stroud, Phys. Rev. B **28**, 2447 (1983).

[22] S. V. Barabash and D. Stroud, Physica B (Amsterdam) **338**, 224 (2003).

[23] S. V. Barabash and D. Stroud, Phys. Rev. B **67**, 144506 (2003).

[24] J. Corson, R. Mallozzi, J. Orenstein, J. N. Eckstein, and I. Bozovic, Nature (London) **398**, 221 (1999).

[25] J. Corson, J. Orenstein, S. Oh, J. O'Donnell, and J. N. Eckstein, Phys. Rev. Lett. **85**, 2569 (2000).

[26] W. Zimmermann, E. H. Brandt, M. Bauer, E. Seider, and L. Genzel, Physica C **183**, 99 (1991).

[27] I. Schürrer, E. Schachinger, and J. P. Carbotte, Physica C **303**, 287 (1998).

[28] J. Hwang, T. Timusk, and G. D. Gu, J. Phys.: Condens. Matter **19**, 125208 (2007).

[29] S. Barabash, D. Stroud, and I.-J. Hwang, Phys. Rev. B **61**, R14924 (2000).

[30] J. Orenstein, Physica C **390**, 243 (2003).

[31] J. H. Han, Phys. Rev. B **66**, 054517 (2002).

[32] J. Corson, J. Orenstein, J. Eckstein, and I. Bozovic, Physica B (Amsterdam) **280**, 212 (2000).

[33] E. J. Nicol and J. P. Carbotte, Phys. Rev. B **71**, 054501 (2005).

[34] J. P. Carbotte, E. Schachinger, and J. Hwang, Phys. Rev. B **71**, 054506 (2005).

[35] W. Götze and P. Wölfle, Phys. Rev. B **6**, 1226 (1972).

[36] T. Mori, E. J. Nicol, S. Shiizuka, K. Kuniyasu, T. Nojima, N. Toyota, and J. P. Carbotte, Phys. Rev. B **77**, 174515 (2008).

[37] J. Hwang, E. J. Nicol, T. Timusk, A. Knigavko, and J. P. Carbotte, Phys. Rev. Lett. **98**, 207002 (2007).

[38] J. Hwang, J. P. Carbotte, and T. Timusk, Phys. Rev. Lett. **100**, 177005 (2008).

[39] H. Tashiro, J. M. Graybeal, D. B. Tanner, E. J. Nicol, J. P. Carbotte, and G. L. Carr, Phys. Rev. B **78**, 014509 (2008).

[40] U. Nagel, D. Hüvonen, E. Joon, J. S. Kim, R. K. Kremer, and T. Room, Phys. Rev. B **78**, 041404(R) (2008).

[41] D. Basov (private communication).